Neuroendocrine tumor in lung

Dr-Ahmed Abu Ryash

Medical paper,

Wenzhou medical university.

❖

❖ Abstract

The majority of neuroendocrine tumeurs in the gastrointestinal tractor and bronchopulmonary system may mature in the human body. The tumours of neuroendocrine are categorised according to the degree of biological aggression (G1–G3) and the degree of differentiation. Typical (G1) and atypical (G2) carcinoids are the well differentiated neoplasms. Largely distinguished neuroendocrine carcinomas in large cells and small cell carcinomas (G3). Identification and distinction of atypical carcinoids or large-cell neuroendocrine carcinomas and small-cell carcinomas in care choices and pronostics is important. The neuroendocrinal pulmonary tumours are distinguished by proportion of necrosis and mitotic activity, palisading, rosetary, trabecular pattern and organic nesting. The information provided on the histopathological evaluation, characterization, prognoses, genetic aberration and treatment options of neuroendocrine pulmonary tumours is based on their own experiences and on an examination of the present literature. In the identity of typical versus atypical carcinoids atypical versus regular, cell neuropheneous, and big neuroendocrine, large cell carcinomas versus small cell carcinomas, there is a majority of differences between classification of neuroendenocrine tumour entities. Of addition, the classification in small biopsies that can be packed into cytological specimens is constrained by the specimen specificity of the immunohistochemical markers and potential objects. To this day, the prevalence of neuroendocrine pulmonary tumours has increased. As compared to NSCLCs, only little research has been done with respect to new molecular targets as well as improving the classification and differential diagnosis of neuroendocrine tumors of the lung.

The origin and tumour development of neuroendocrine neoplasms, also known as epithelial neoplasms with neuroendocrine differentiation, are debated, but most researchers agree that these tumours arise from Kulchitzky cells (or enterochromaffin cells, which are normally found

in the bronchial mucosa) as part of the diffuse neuroendocrine system, which consists of single cells or cluste. **(Rekhtman, 2010).**

Neuroendocrine tumours (NETs) account for 20–25 percent of all invasive lung cancers, while non-small cell lung cancer accounts for 75 percent (NSCLC). Siegfried Oberndorfer first identified neuroendocrine tumours as carcinoid tumours in 1904, and they form from hormone-producing (endocrine) cells located in the following body regions: **(Travis, 2010).**

- Foregut: Thymus, lung, bronchi, trachea,
- Midgut: Small intestine, gallbladder, pancreas,
- Hindgut: Colon, excluding appendix, rectum,

Tumors have properties that are similar to those in neurons. As a result, they're called neuroendocrine tumours. However, only about a third of these tumours are inactive (no hormone production). Secretory capacities to pick up and decarboxylate amine precursors are also present in neuroendocrine lung tumours (APUD system cells). NETs of the lungs, according to the World Health Organization (WHO) classification of 2004, have morphological, immunohistochemical, and molecular characteristics in general and can be divided into three groups: **(Valente et al., 2010).**

- Carcinoid tumors (typical (TC)/atypical (AC)),
- Large cell neuroendocrine carcinomas (LCNEC),
- Small cell carcinomas (SCLC).

These neuroendocrine entities are further summarized into two groups according to their biological aggressiveness:

- Well-differentiated low grade (G1) typical and intermediate grade (G2) atypical carcinoids,
- Poorly-differentiated high grade (G3) LCNEC and SCLC.

In contrast to typical and atypical carcinoids, LCNEC and SCLC are not closely related to each other regarding genetic and epigenetic characteristics. Contrary to carcinoids, no precursor lesions are known for SCLCs and LCNECs

❖ Epidemiology

Neuroendocrine tumours rise in frequency in a linear fashion. Neuroendocrine tumours account for just 0.5–2% of all cancers diagnosed in adults. Patients with carcinoid tumours are considerably younger than patients with SCLC and LCNEC (the majority of whom are men). **(Faggiano and colleagues, 2012).**

Nearly all patients with SCLC (95 percent of all SCLC occur in the bronchial system) and LCNEC are heavy cigarette smokers. Carcinoids (AC 0.1–0.2%), 3.0% LCNEC, 15–20.0 percent SCLC, and 75–80 percent non-neuroendocrine carcinomas make up 1–2.0 percent of lung tumours.Patients with inherited autosomal-dominant syndrome of multiple endocrine neoplasia type I (MEN I) and other hereditary histories show a higher incidence of malignant neuroendocrine lesions. **(Taal & Visser, 2004).**

❖ Clinical Features

Clinical characteristics are determined by the tumor's position and biological aggressiveness. Recurrent infections, chest pain, cough, dyspnea, and pneumonia are all possible symptoms of centrally located carcinoids. The ones that are found on the periphery are usually unintentional.

Carcinoids, unlike high-grade NETs, appear in around 5% of patients with hereditary multiple neuroendocrine neoplasia. While well-differentiated neuroendocrine lesions may produce hormones similar to those produced by the nervous system, lung carcinoids are rarely associated with hypersecretion and paraneoplastic syndromes when compared to gastroenteropancreatic NETs. The carcinoid syndrome and Cushing's Syndrome are predominately found in carcinoids and are only rare for patients with LCNECs or SCLCs. **(Rekhtman, 2010).**

❖ Carcinoid Tumors

Carcinoid tumours of the lungs or bronchi account for more than 25% of all carcinoid tumours and 1%–2% of all pulmonary neoplasms. Atypical carcinoids make up about 10%–20% of pulmonary carcinoids, while typical carcinoids make up the remaining 80%–90%. The majority of these tumours (60–70%) occur centrally and affect the primary, lobar, or segmental airways. Modlin et al. **(Modlin et al., 2003).**

Women are believed to be significantly more susceptible to these tumours than men. However, some researchers have recently discovered that carcinoids can affect both males and females equally, or may have a male predominance with a male-to-female ratio of up to 3.6:1. Atypical carcinoids are more commonly found in males.The mean presenting age is 46 years with a wide age range. Patients with carcinoid tumors are younger than those with common primary lung cancer. **(Chong et a., 2006).**

Since centrally located tumours are more likely to be normal carcinoids than atypical carcinoids, central airway obstruction symptoms and signs appear earlier than peripherally located atypical carcinoids. As a result, atypical carcinoids patients are around ten years older than people with standard carcinoids (59 years in atypical carcinoids and 49 years in typical carcinoids). Carcinoids are the most common primary pulmonary neoplasm in infants, with the majority of cases occurring in late adolescence. Coughing, wheezing, and hemoptysis are common presenting symptoms of bronchial obstruction. However, about 25% of patients are asymptomatic, and thus bronchial carcinoids may be found incidentally. **(Detterbeck, 2010).**

Atypical carcinoids, unlike traditional carcinoids, are linked to a history of cigarette smoking (83–94 percent of cases) and are more common in men (2:1). The majority of traditional carcinoids (80–90%) are stage I cancers, while about half of atypical carcinoids are stage I cancers. Lobectomy and pneumonectomy are the most common therapies for carcinoid tumours. Typical carcinoids and atypical carcinoids have 5-year survival rates of 87 percent and 56 percent, respectively, and the survival rate for atypical carcinoid is slightly lower than that of typical carcinoid **(Chong et al., 2006).**

- **Histologic Findings**

Histologic characteristics are used to differentiate between typical and atypical carcinoids. Small nests or interconnecting trabeculae of uniform cells are found in both tumours, which are divided by a prominent vascular stroma and multiple thin-walled blood vessels (Figs 1,2). Atypical carcinoids have areas of necrosis or 2–10 mitoses per 10 high-power fields (HPFs) (or 2 mm2) of viable tumour, while normal carcinoids have no evidence of necrosis and less than 2 mitoses per 10 HPFs (or 2 mm2) of viable tumour. **(Ferlito et al., 2009).**

Typical carcinoids and atypical carcinoids also have dense core granules in the cytoplasm that are homogeneous in size, but typical carcinoids have more of them and they are usually larger than atypical carcinoids. Neurosecretory granule immunohistochemistry is typically diffuse, with standard carcinoids showing the highest percentages, distributions, and intensities. Panneuroendocrine markers such as neuron-specific enolase, chromogranin, and synaptophysin are useful for recognising neuroendocrine features but have no bearing on the diagnosis or prognosis of a pulmonary neuroendocrine tumour. **(Valli et al., 1994).**

The histopathologic features that distinguish atypical carcinoid from typical carcinoid are as follows:

a) increased mitotic activity,
b) greater cytologic pleomorphism and higher nuclear-to-cytoplasmic ratios,
c) increased cellularity and architectural irregularities,
d) more areas of tumor necrosis.

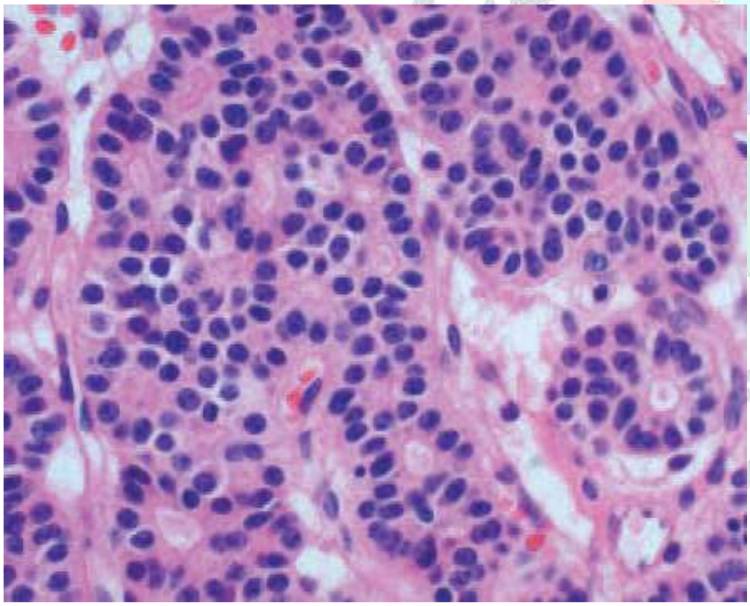

Figure 1. Typical carcinoid. Photomicrograph (original magnification, 100; hematoxylin-eosin stain) shows small nests of uniform cells.

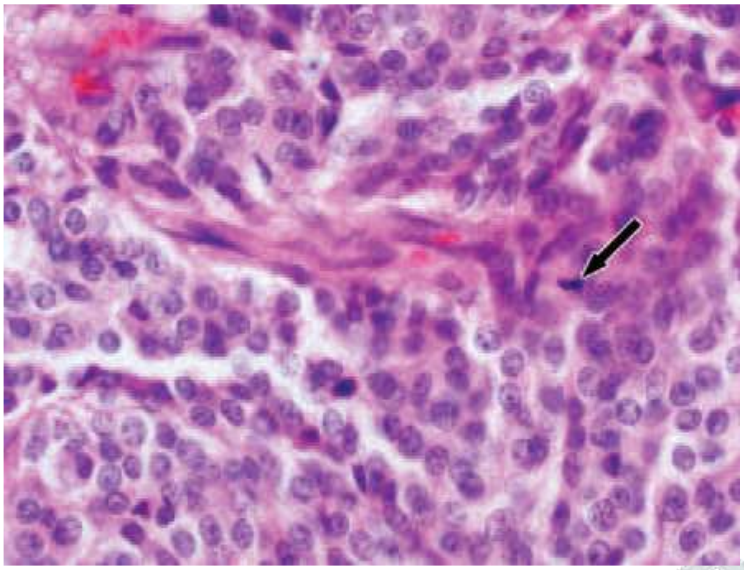

Figure 2. Atypical carcinoid. Photomicrograph (original magnification, _400; hematoxylin-eosin stain) shows nuclear pleomorphism and mitosis (arrow).

- **Imaging Findings**

The imaging characteristics of normal and atypical carcinoids are too similar to be distinguished. While carcinoids are found in a variety of locations, the majority are centrally located and thus associated with airways. The peripheral lung accounts for 16–40% of all cancers. A well-defined hilar or perihilar mass (Fig 3) is most often seen on chest radiographs as an isolated finding or with associated distal parenchymal disease. Consolidation of the parenchyma may be present, indicating atelectasis, obstructive pneumonitis, or persistent pneumonia (Fig 4). Mucus plugging, which appears as a "gloved finger" pattern when several contiguous bronchi are dilated, may be the cause. **(Caplin and colleagues, 2015).**

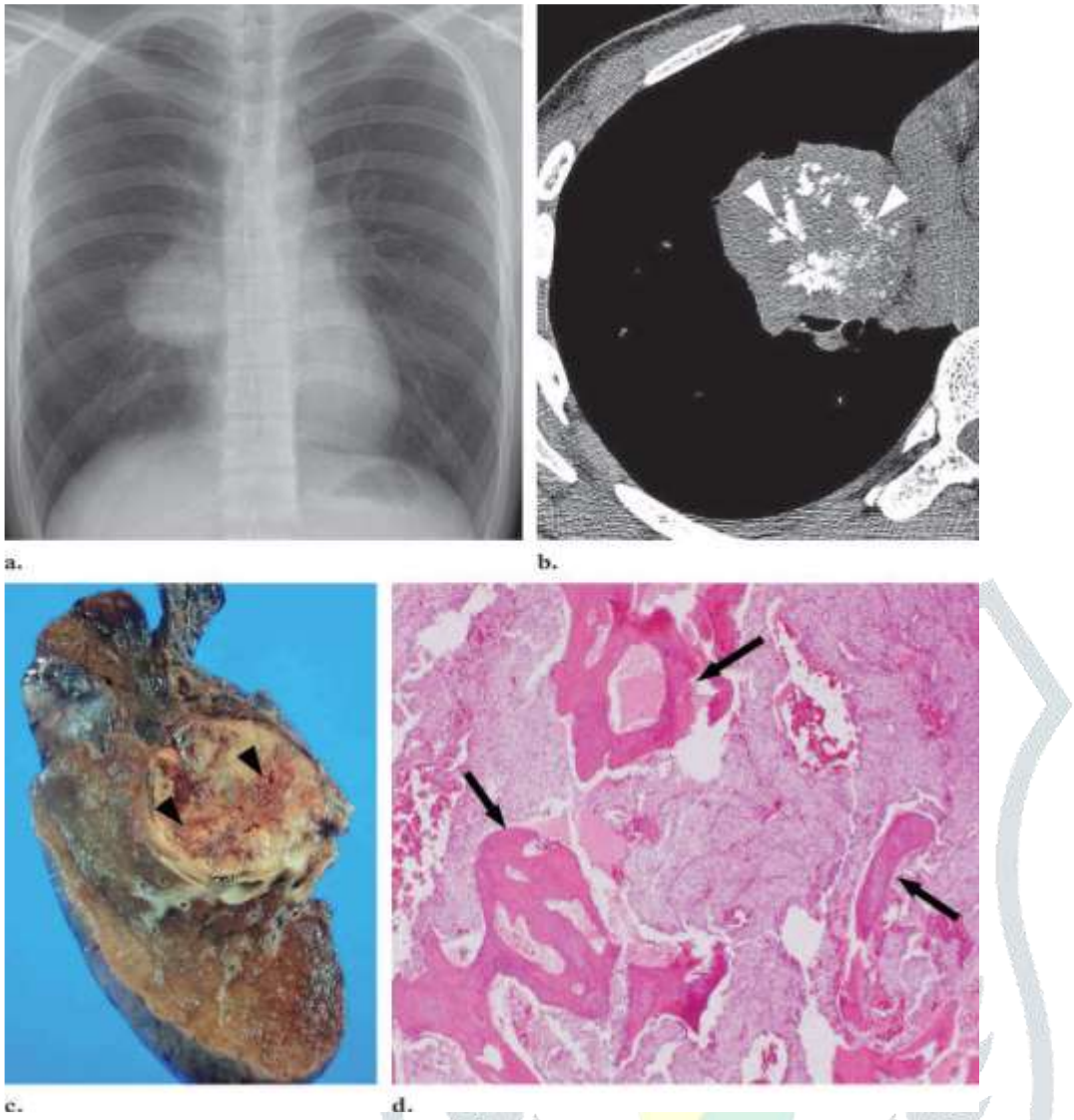

Figure 3. This is a typical carcinoid. (a) A lobulated mass below the right hilum is visible on a chest radiograph. (b) Axial thin-section computed tomographic (CT) scan of the right middle lobe (1.0-mm section thickness) reveals a massive (60-mm-diameter) mass with punctate calcifications (arrowheads). (c) A gross specimen obtained via right lobectomy reveals a broad endobronchial mass with central ossification (arrowheads). (d) Photomicrograph of metaplastic bone (arrows) in the tumour (original magnification, _100; hematoxylin-eosin stain).

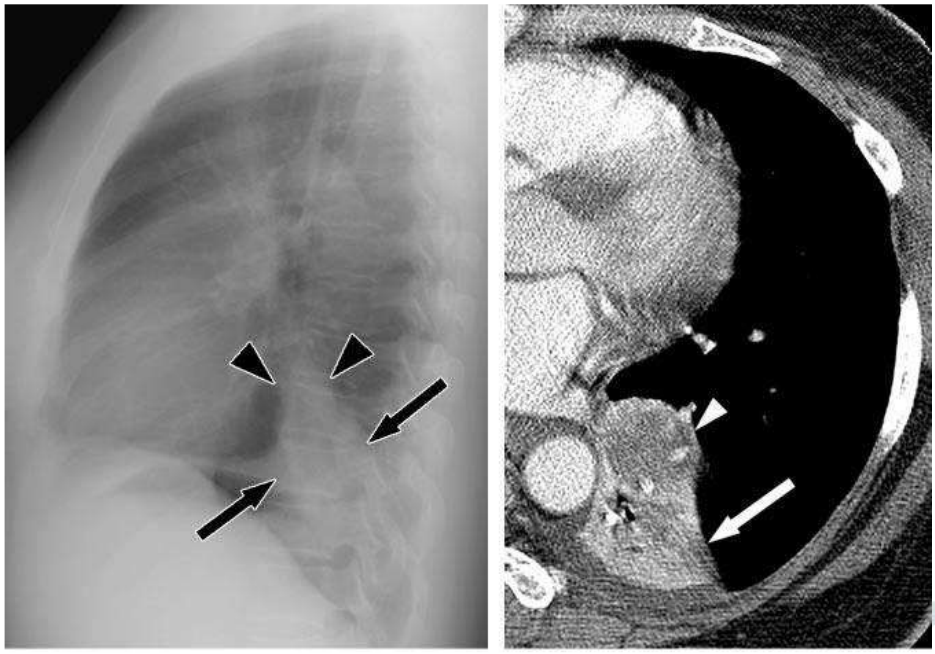

a. b.

Figure 4. a typical carcinoid. (a) A lateral chest radiograph reveals left lower lobe atelectasis (arrows) and a central mass (arrowheads). (b) Axial CT scan at the level of the left atrium (5.0-mm segment thickness) reveals a 20-mm-diameter endobronchial nodule (arrowhead) in the left basal trunk, as well as atelectasis of the left lower lobe (arrow).

Carcinoid tumours may sometimes be found distal to segmental bronchi; these tumours are known as peripheral carcinoids. There are well-defined round or ovoid lesions with lobulated margins that are less than 3 cm in diameter (Fig 5) and are well-defined round or ovoid lesions with lobulated margins. Atypical carcinoids are larger than normal carcinoids, with mean diameters of 3.6 cm and 2.3 cm, respectively, and are more likely to occur in the periphery of the lung than typical carcinoids. Metastases affect 15% of bronchial carcinoids and are most commonly found in the liver, bone, adrenal glands, and brain. **(Saoud and colleagues, 2016).**

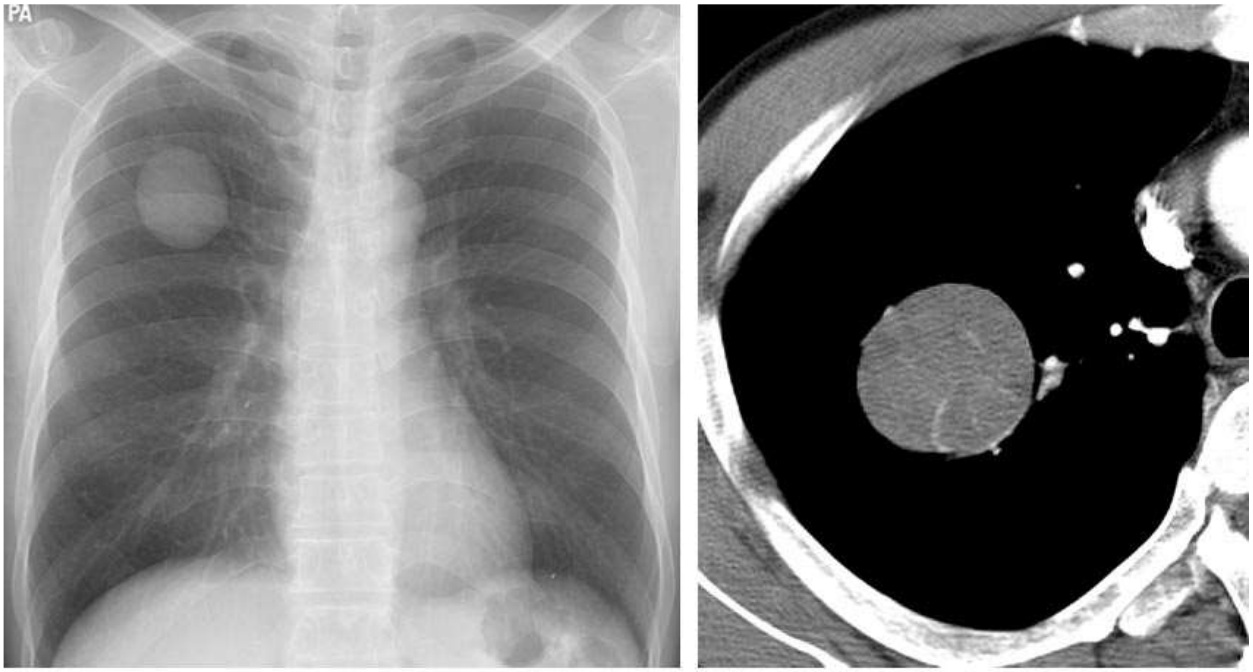

Figure 5. Typical carcinoid (a) Chest radiograph shows a well-defined round mass in the right upper lobe. (b) Axial CT scan (5.0-mm section thickness) obtained with a mediastinal window shows the homogeneous mass.

Carcinoid tumours are visualised on CT as a spherical or ovoid nodule or mass with a well-defined and slightly lobulated margin. The tumours have an elongated appearance because they are nonspherical, with the long axis parallel to neighbouring bronchi or pulmonary artery branches. They are usually found near the bifurcation region of the central bronchi (Figs 6, 7). Calcification is rarely apparent on chest radiographs, but calcification or ossification can be seen in up to 30% of tumours on CT images (Fig 3) and can appear in a punctate or diffuse pattern. Furthermore, core carcinoids calcify more often than peripheral carcinoids.Therefore, observation of a central tumor that causes narrowing, deformation, or obstruction of a bronchus and that displays punctate or diffuse calcification should suggest the diagnosis of bronchial carcinoid (Fig 3). **(Baxi et al., 2017).**

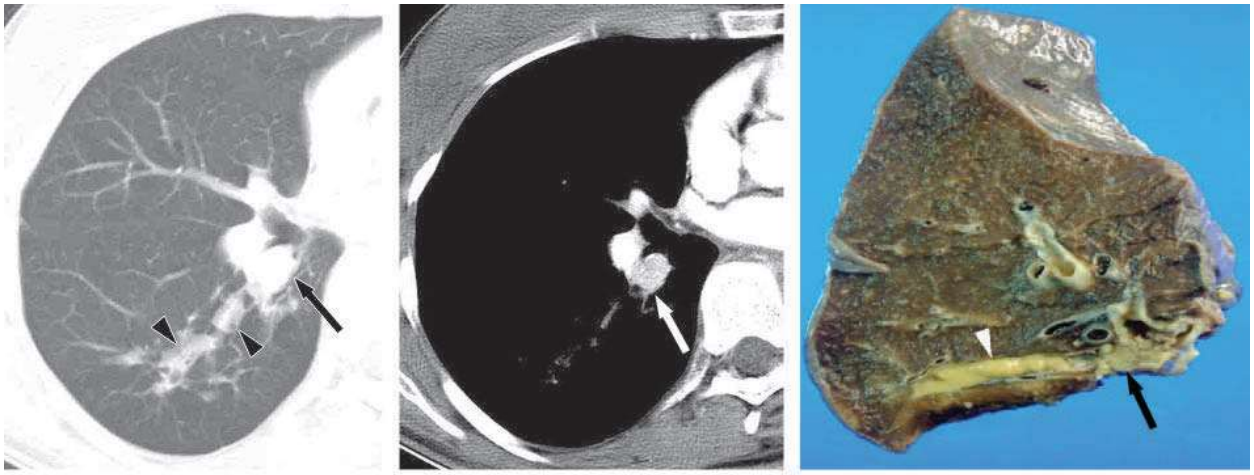

Figure 6. this is a typical carcinoid. (a) Axial CT scan at the level of the right middle lobar bronchus reveals a 13-mm-diameter nodule (arrow) in the superior segmental bronchus of the right lower lobe with distal mucus plugging (arrowheads). (b) The endobronchial nodule is significantly enhanced when viewed through a mediastinal window on the same image (arrow). The yellow polypoid endobronchial nodule is visible in the gross specimen (c) (arrow). Take note of the mucus plugging at the distal end (arrowhead).

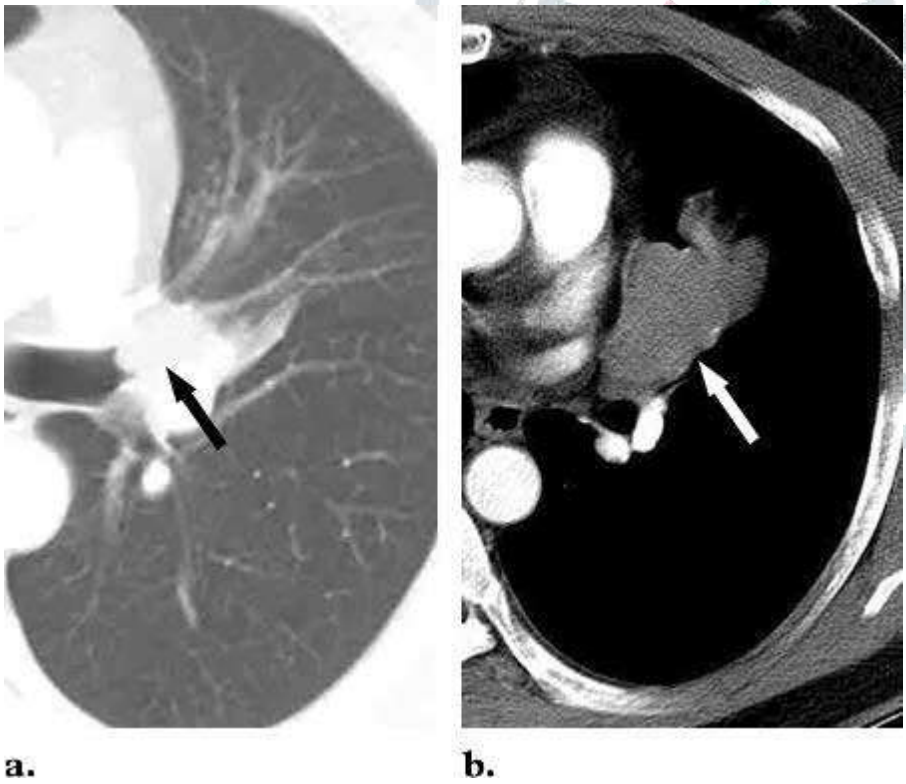

Figure 7 a typical carcinoid. (a) Axial CT scan at the level of the distal left main bronchus (5.0-mm segment thickness) reveals a nodule (arrow) in the left upper divisional bronchus. The low-attenuation mass (arrow) in the lingular segmental bronchus is visible on a CT scan (mediastinal window) obtained 10 mm inferior to a. There was no atelectasis or obstructive pneumonia present.

Carcinoids may often appear as a small nodule entirely inside a bronchus' lumen (Figs 6, 7). The bronchial relationship between the tumour and the bronchus can be assessed using thin-section CT. Where a small nodule abuts a subsegmental bronchus or a small endoluminal portion of the tumour is visible on thin-section CT, even a small nodule located beyond the origin of a subsegmental bronchus can be observed. Although the endoluminal component may or may not be visible on CT (Figs 6, 8), the intraluminal component may be small in comparison to the bulk of the tumour, so it is just the tip of the iceberg when seen (Fig 8). Peripheral carcinoids may manifest as a well-defined, lobulated nodule or mass without evidence of a bronchial relationship at CT (Fig 5). **(Benson et al., 2013).**

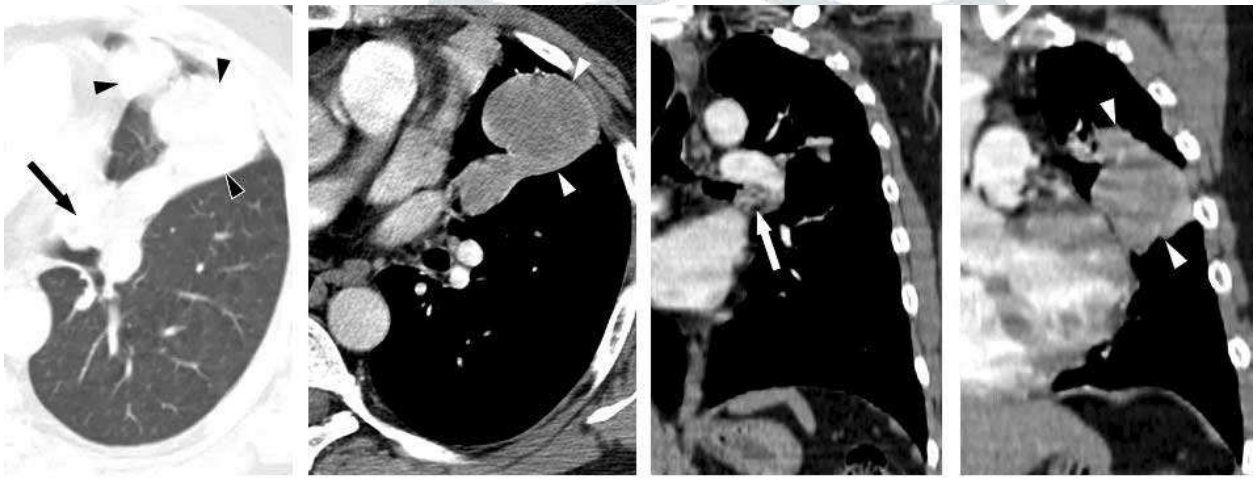

Figure 8. a typical carcinoid. (a) Axial CT scan at the level of the left lower lobar bronchus (2.5-mm section thickness) reveals a multilobulated mass in the lingular segmental bronchus and at the lingular division. The mass is made up of both endobronchial (arrow) and extrabronchial (arrowheads) elements, resulting in an iceberg tumour. The slightly heterogeneous parenchymal mass (arrowheads) at the lingular division is visible on a CT scan (mediastinal window) obtained 10 mm inferior to a. (c, d) Coronal reformatted images (2.5-mm segment thickness) demonstrate the tumor's endobronchial (arrow in c) and extrabronchial (arrowheads in d) components.

Carcinoids are vascular and can provide a lot of enhancement (Fig 6). This is especially useful for separating the tumour from obstructive atelectasis or a mucus plug in the same area. In a dynamic contrast-enhanced CT sample, both typical and atypical carcinoid (Figs 9 and 10) show high enhancement, with more than 30 HU of net enhancement in both cases. Both standard and atypical carcinoids have been linked to hilar or mediastinal lymphadenopathy as a result of

recurrent pneumonia-induced reactive hyperplasia or lymph node metastasis. Atypical carcinoids are more likely to cause lymph node metastases. **(Park et al., 2009).**

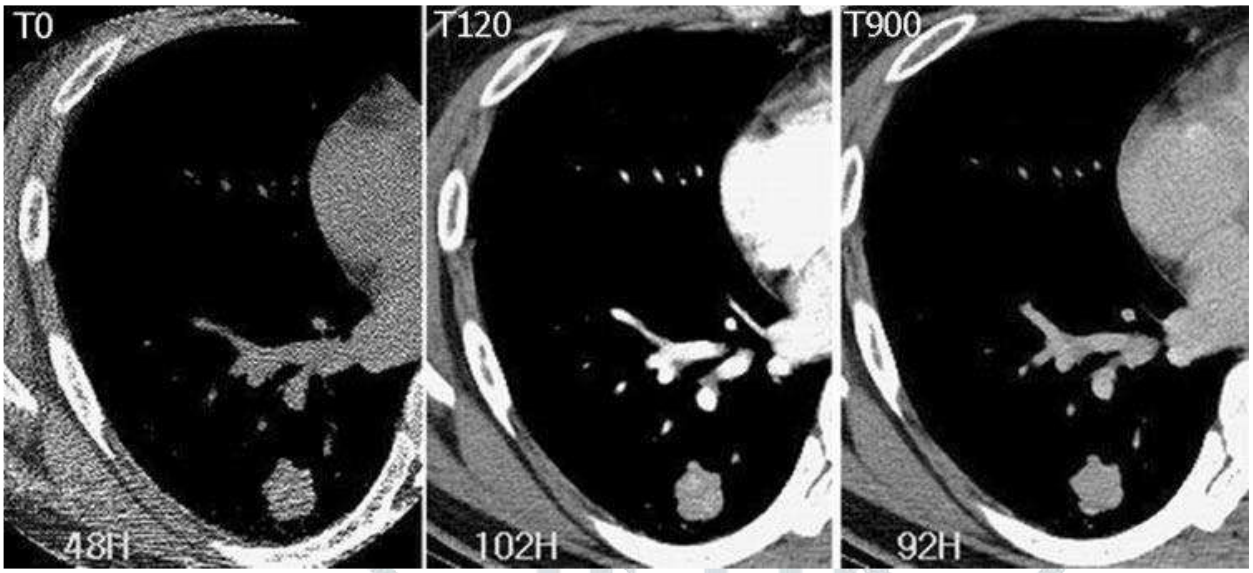

Figure 9. a typical carcinoid. After intravenous injection of 120 mL of contrast medium (iodine concentration, 36 g), dynamic contrast-enhanced CT scans (2.5-mm segment thickness) reveal an 18-mm-diameter enhancing nodule in the right lower lobe. On the unenhanced image (T0), the nodule attenuates 48 HU, 102 HU (54 HU of net enhancement) on the 2-minute image (T120), and 92 HU (10 HU of washout) on the 15-minute image (T120) (T900).

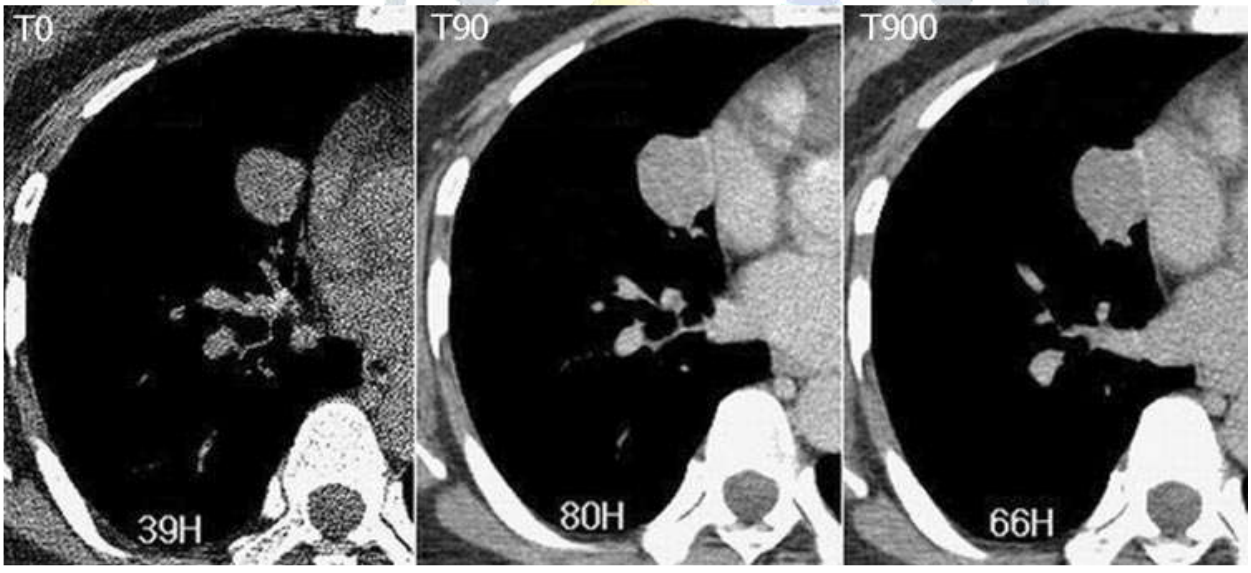

Figure 10. atypical carcinoid. After intravenous injection of 120 mL of contrast medium (iodine concentration, 36 g), dynamic contrast-enhanced CT scans (2.5-mm segment thickness) reveal a 28-mm-diameter enhancing nodule in the right middle lobe. On the unenhanced image (T0), the nodule attenuates by 39 HU, 80 HU (41 HU of net enhancement) on the 90-second image (T90), and 66 HU (14 HU of washout) on the 15-minute image (T15) (T900).

Carcinoid tumors have high numbers of somatostatin receptors, which allow scintigraphic imaging with the radiolabeled somatostatin analog octreotide. Accordingly, octreotide scanning has been found to be helpful for detecting occult tumors, particularly those with paraneoplastic symptoms. At positron emission tomography (PET) performed with fluorine 18 fluorodeoxy-glucose (FDG), most carcinoid tumors do not exhibit increased activity (Fig 11) and usually have lower FDG uptake than expected for malignant tumors. However, it was recently reported that carcinoid tumors show increased FDG uptake and thus high metabolic activity and malignant potential. We have also observed increased FDG uptake in atypical carcinoid (Fig 12). Therefore, conservative management such as follow-up imaging should be performed only when PET shows no or little FDG uptake, although results of imaging studies suggest carcinoid tumors. **(Volante et al., 2007).**

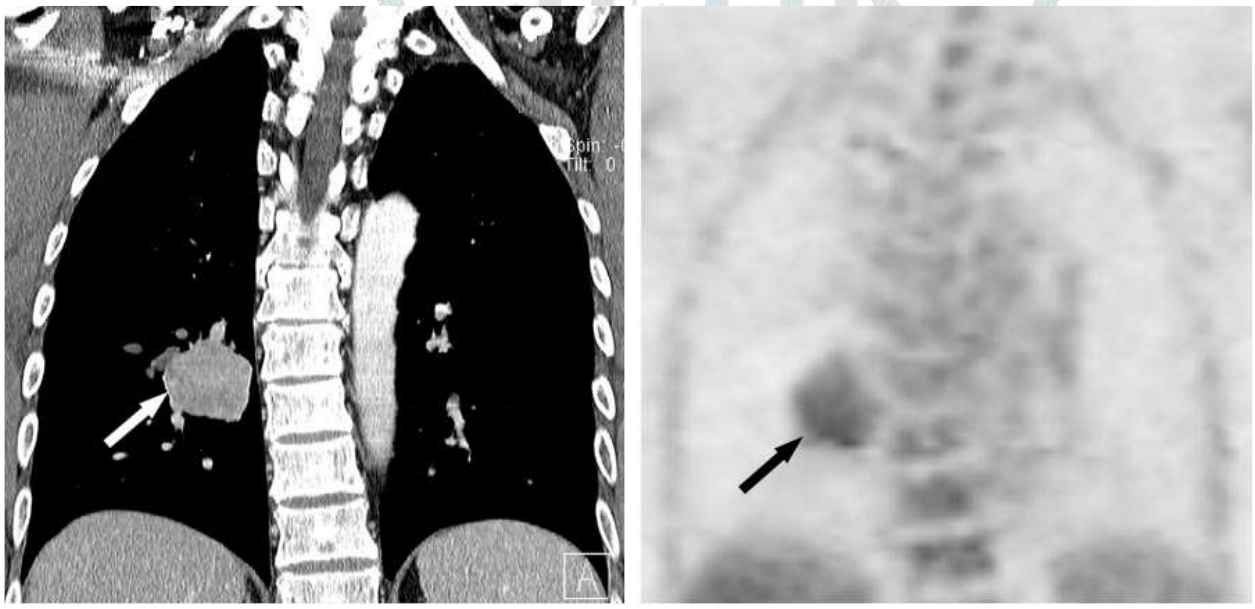

a. b.

Figure 11. Typical carcinoid (a) Coronal reformatted image (2.5-mm section thickness) shows a 41-mm-diameter, moderately enhancing, homogeneous mass (arrow) in the right lower lobe. (b) On a PET image, the mass demonstrates little FDG uptake (arrow).

❖ Large Cell Neuroendocrine Carcinoma

Because of its clinical and pathologic differences from standard carcinoid, atypical carcinoid, and SCLC, LCNEC was recently proposed as the fourth type of pulmonary neuroendocrine tumours. LCNEC is a poorly differentiated, high-grade neuroendocrine tumour that resembles atypical carcinoid and SCLC morphologically. Patients range in age from 60 to

80 years old, and men are much more likely than women to be involved (more than 2.5 times). Smoking is prevalent among the patients, with more than 60% of them being smokers. The clinical characteristics of LCNEC, as well as the best treatment options, have yet to be determined. **(Battafarano and colleagues, 2005).**

LCNEC is found in 2.9 percent of surgically resected lung cancers, 19 percent of pulmonary neuroendocrine tumours, and 12 percent of all large cell undifferentiated carcinomas, according to studies. According to many studies, the prognosis for LCNEC is low, with a 5-year survival rate ranging from 13 percent to 45 percent. Takei et al observed no substantial difference in overall survival between patients with LCNEC and those with other poorly differentiated non–small cell lung cancers (NSCLCs) in a study of 87 patients with LC-NEC; however, a slightly worse (P =.003) difference in survival was found between patients with stage I LCNEC and those with other poorly differentiated non–small cell lung cancers (NSCLCs) (67 percent 5-year survival rate) and those with the same stage of other poorly differentiated NSCLCs (88% 5-year survival rate). In a recent 10-year clinicopathologic study, Paci et al reported that LCNEC has a poorer prognosis than NSCLC, even at an early stage, with an overall 5-year survival rate of 21%. **(Miyoshi et al., 2017).**

- **Histologic Findings**

The diagnosis of LCNEC has been established by histologic and cytologic evaluations, immunohistochemistry, or electron microscopy. The World Health Organization (WHO) proposed histopathologic diagnostic criteria for LCNEC: **(Travis, 2014).**

a) neuroendocrine morphologic features (organoid nesting, palisading, rosettes, or a trabecular growth pattern) (,Fig 13);
b) a high mitotic rate (> 10 per 10 HPFs);
c) necrosis (often large zones);
d) cytologic features different from those of SCLC (large cell size, polygonal shape, a low nuclear-cytoplasmic ratio, finely granular eosinophilic cytoplasm, coarse nuclear chromatin, and frequent nucleoli);

e) positive immunohistochemical staining for one or more neuroendocrine markers including chromogranin A, synaptophysin, and neural cell adhesion molecule (NCAM/CD56).

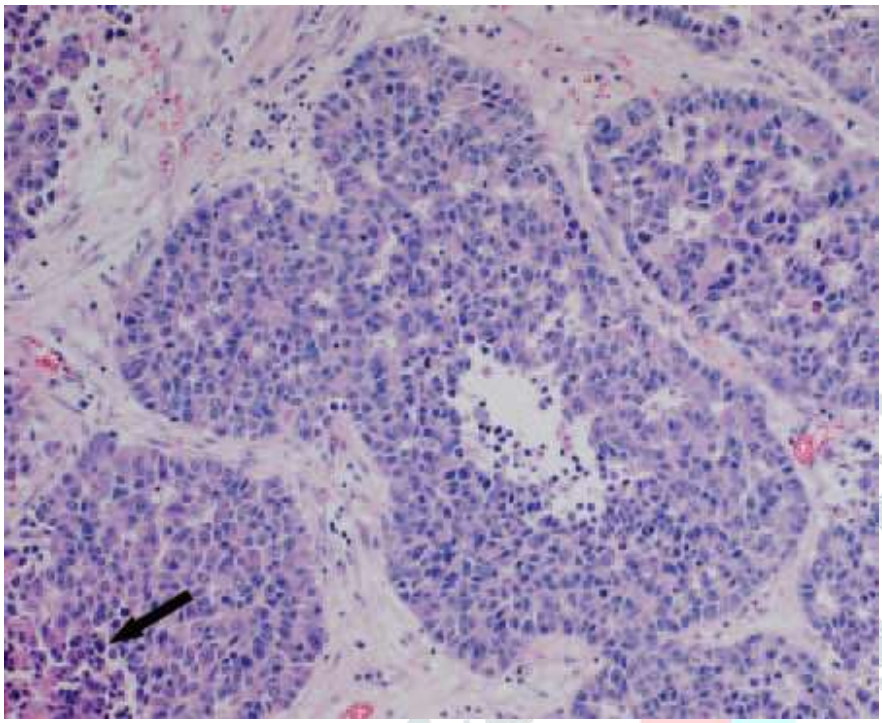

Figure 13. LCNEC is an abbreviated form of LCNEC. A neuroendocrine presence with peripheral palisading and rosettes can be seen in this photomicrograph (original magnification, 100; hematoxylin-eosin stain). Take note of the necrosis (arrow). Since transthoracic fine-needle aspiration or biopsy diagnosis may be difficult, clinicopathologic or radiologic findings studies should only involve cases of surgically resected LCNEC.

The histologic criteria for LCNEC differ from those for atypical carcinoid mainly in two ways: (a) LCNEC has more frequent mitoses (> 10 per 10 HPFs) than atypical carcinoid (2–10 per 10 HPFs), and (b) LCNEC has a lower nuclear-cytoplasmic ratio than atypical carcinoid. **(Tsuta et al., 2011).**

- **Imaging Findings**

LCNEC's radiologic findings are close to those of other traditional NSCLCs, despite the fact that they have not been recorded in depth. LCNEC was not included in Forster et al's definition of the spectrum of radiologic changes in neuroendocrine carcinomas of the lung since their analysis was published before the WHO classification proposal. The radiologic findings of LCNEC can also be hypothesised to be intermediate between those of atypical carcinoid and

those of SCLC, according to the WHO suggestion that the morphologic features of LCNEC reflect a continuum between those of atypical carcinoid and those of SCLC **(Cueto et al., 2014).**

Eight of the 11 tumours studied by Jung and colleagues (73%) manifested as a peripheral mass or nodule (Figs 14–17), while three tumours (27%) manifested as a central mass with attendant atelectasis or distal mucus plugging (Fig 18). Over the course of the 15-month follow-up period, three of 11 patients (27%) had mediastinal lymph node enlargement (Fig 16), and four patients (36%) had extrathoracic metastasis. The CT results of LCNEC of the lung are nonspecific and close to those of other NSCLCs, according to the scientists. Similarly, in the study by Oshiro et al, 32 of 38 tumours (84%) were located peripherally, while six (16%) were located centrally. Katyal and colleagues **(Katyal et al., 2000).**

Nodules or masses are usually well-defined and lobulated (Figs 14–17), but they may also have a spiculated margin. Air bronchogram, cavity, bubble lucency, or necrosis are some of the internal features of nodules or masses that can be seen on CT. 9 percent of patients with LCNEC have intratumoral calcifications. A pleural tag or surrounding emphysema are two other possible findings. Tumor attenuation on contrast-enhanced CT scans ranges from slightly less to slightly more than the chest wall muscle, with a homogeneous or heterogeneous pattern. Necrotic foci can be found in almost all tumours. At enhanced CT, massive tumours appear with heterogeneous attenuation. whereas small tumors do not necessarily show heterogeneous attenuation despite the presence of necrotic foci histopathologically (Figs 15, 17). Pleural effusion is observed in 24% of cases. **(Zhang & Zheng, 2018).**

There has been no study on PET imaging of LCNEC. We have some experience with PET study of LCNEC. The tumors showed avid FDG uptake at PET (Fig 17).

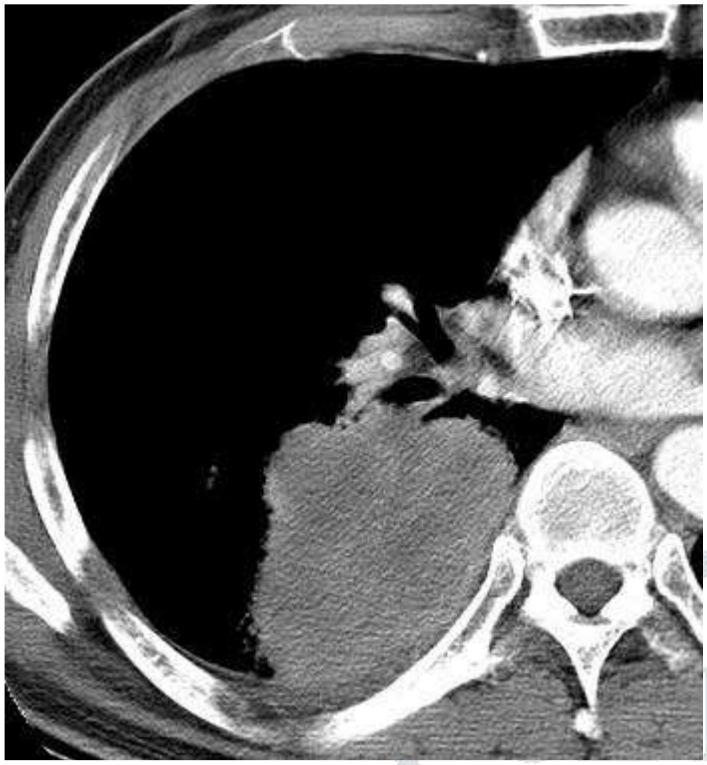

Figure 14. LCNEC Axial CT scan (5.0-mm section thickness) obtained at the level of the right middle lobar bronchus shows a well-defined, 8-cm-diameter mass abutting the chest wall in the right lower lobe.

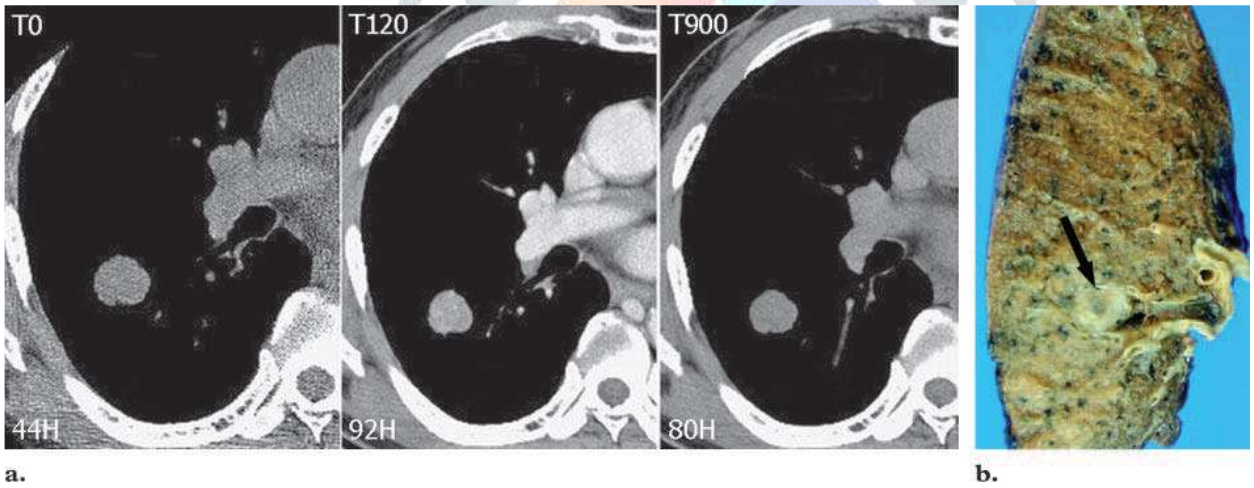

Figure 15. LCNEC. (a) Dynamic contrast-enhanced CT scans (2.5-mm segment thickness) display a 23-mm-diameter peripheral nodule in the right lower lobe following intravenous injection of 120 mL of contrast medium (iodine concentration, 36 g). On the unenhanced image (T0), the nodule attenuates 44 HU, 92 HU (48 HU of net enhancement) on the 2-minute image (T120), and 80 HU (12 HU of washout) on the 15-minute image (T900). (b) A well-defined, whitish tan, soft nodule is visible in the pathologic specimen (arrow).

a. b.

Figure 16. LCNEC. (a) A 32-mm-diameter mass with a lobulated margin in the right upper lobe is seen on an axial CT scan (5.0-mm section thickness) obtained at the level of the thoracic inlet. (b) An swollen lymph node at the right lower paratracheal region (arrowhead) and at the right hilum can be seen on a CT scan taken at the level of the right upper lobar bronchus (arrow). Malignant cells were found in the right lower paratracheal nodes during a mediastinoscopic

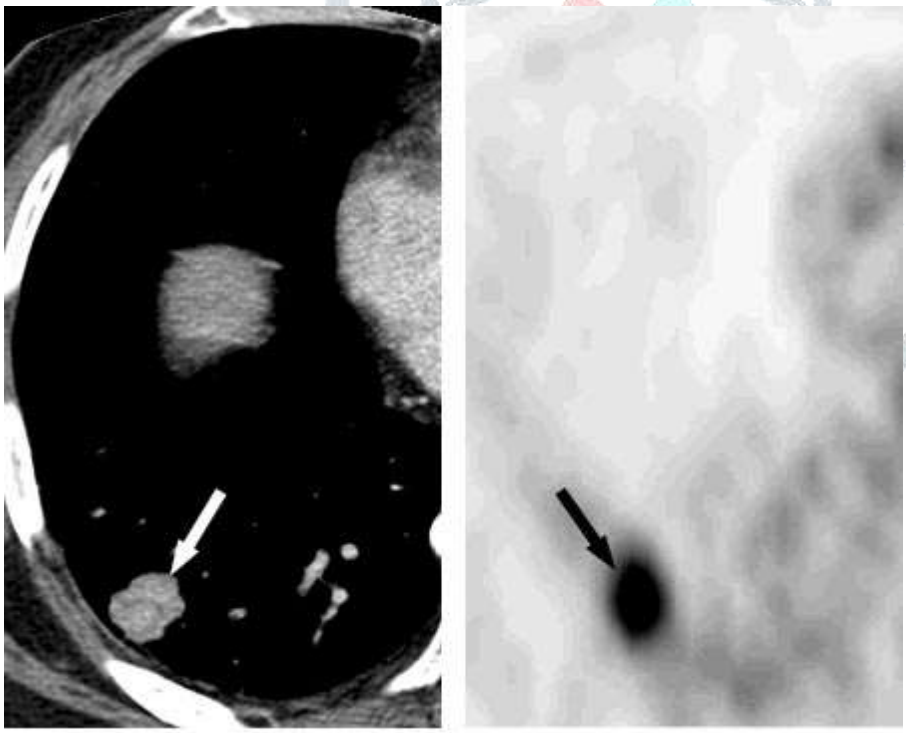

study. **a.** **b.**

Figure 17. LCNEC (a) Axial CT scan (5.0-mm section thickness) obtained at the level of the hepatic dome shows a 20-mm-diameter nodule (arrow) in the right lower lobe. (b) Axial PET image shows that the nodule (arrow) is hypermetabolic (peak standardized uptake value 8.2).

❖ Small Cell Lung Cancer

SCLC makes up approximately 20% of all bronchogenic carcinomas. SCLCs appear to originate in a lobar or key bronchus in 90–95 percent of cases. SCLC patients are on average about 70 years old. Tobacco use is more closely linked to SCLC than any other form of histologic cancer. Dyspnea, a chronic cough, hemoptysis, and postobstructive pneumonia are all common clinical symptoms. Dysphagia, hoarseness, and superior vena cava syndrome can result from the invasion of adjacent structures. Patients typically have severe disease and accelerated tumour development before they are diagnosed. **(Gallego et al., 2012).**

SCLC is normally divided into two stages: minimal disease and extensive disease. A tumour restricted to one hemithorax, including regional mediastinal and supraclavicular lymph nodes, is classified as limited disease, while extensive disease is defined as disease that extends beyond these boundaries. The conditions for these two groups, though, are also up for debate. **(Kalemkerian, 2011).**

Patients with primary tumour and nodal presence restricted to one hemithorax are classified as having limited disease by the Veterans Administration Lung Study Group (VALG). The International Association for the Study of Lung Cancer (IASLC), on the other hand, believes that selective illness can also cover all patients who do not have remote metastasis. As a result, the IASLC definition has more patients in the disorder group with a higher prognosis than the VALG definition. About 60%–70% of patients with SCLC who are first diagnosed have advanced disease, and the most common meta-static sites at diagnosis are bone (19%–38%), the liver (17%–34%), the adrenal glands (10%–17%), and the brain (up to 14%). **(Stinchcombe & Gore, 2010).**

Limited disease is treated with combination chemotherapy and concurrent thoracic radiation therapy, whereas extensive disease is treated with chemotherapy alone; any radiation therapy in such cases is performed for symptom palliation.

➢ Histologic Findings

The tumor cells are usually small with a round or fusiform shape and have high cellularity with a very high mitotic rate (Fig 19). The architecture of the tumor clusters is poorly preserved, with

large areas of necrosis separating small islands of viable tumor. At immunohistochemical study, neurosecretory granules such as chromogranin and synaptophysin are usually present, but these are fewer and smaller than those observed in carcinoid tumors

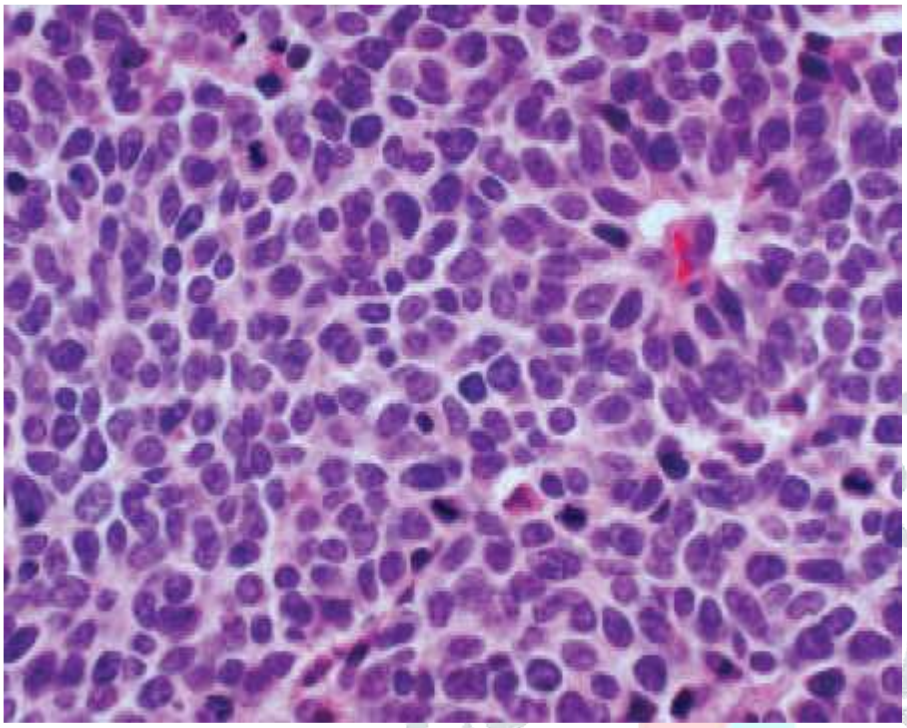

Figure 19. SCLC. Photomicrograph (original magnification, 400; hematoxylin-eosin stain) shows high cellularity; the small round cells have scanty cytoplasm and coarse chromatin. Note the frequent mitoses.

- **Imaging Findings**

Most SCLCs are centrally situated and manifest as mediastinal (92%) or hilar (84%) lymphadenopathy (Figs 20, 21), with tracheobronchial tree (68%) or main vessel displacement or narrowing (68 percent). Some intracardiac CT observations include significant (at least lobar) atelectasis (30%), a noncontiguous parenchymal mass (41%), and pleural effusion (Fig 22). (38 percent). SCLC presents as a peripheral nodule without associated lymphad-enopathy in 5%–10% of instances (Fig 22). In up to 23% of SCLCs, intratumoral calcification can be observed. **(Linning et al., 2019).**

Most peripheral SCLCs are a well described homogeneous mass with lobulation, marginal opacity of the floor glass and conjecture. The marginal opacity of the ground-glass is histopathologically consistent with focal eden and haemorrhage, with an intraalveolar invasion

less common. Fine spiculation is the same as vascular or lymphatic invasion or intraalveolar abnormal expansion. However, those results are unlike the NSCLC findings. **(Cancellieri & Dalpiaz, 2017).**

The peripheral SCLCs are also similar to those of the NSCLCs in dynamically improved contrast CT (Fig 23). This improvement represents inherent tumour angiogensis and is presumed to be vulnerable to proper chemotherapy by a high bloodstream tumour. The further improved a tumour is at CT, the greater its response to chemotherapy is and scientifically Choi and al. recommended a 30 HU tumour increase as a guideline for chemotherapy reaction. **(Kim et al., 2012).**

The use of FDG PET for the assessment of NSCLC has been recorded for SCLC in a small number of studies. Pandit et al indicated that SCLC detection sensitivity of PET is 100 per cent and that a high standardised value of uptake is significantly linked to poor survival (Fig 20). Initial tumour (small vs. extensive) staging and clinical preparation in patients with alleged limited stage diseases are also worth for PET. **(Lee et al., 2009).**

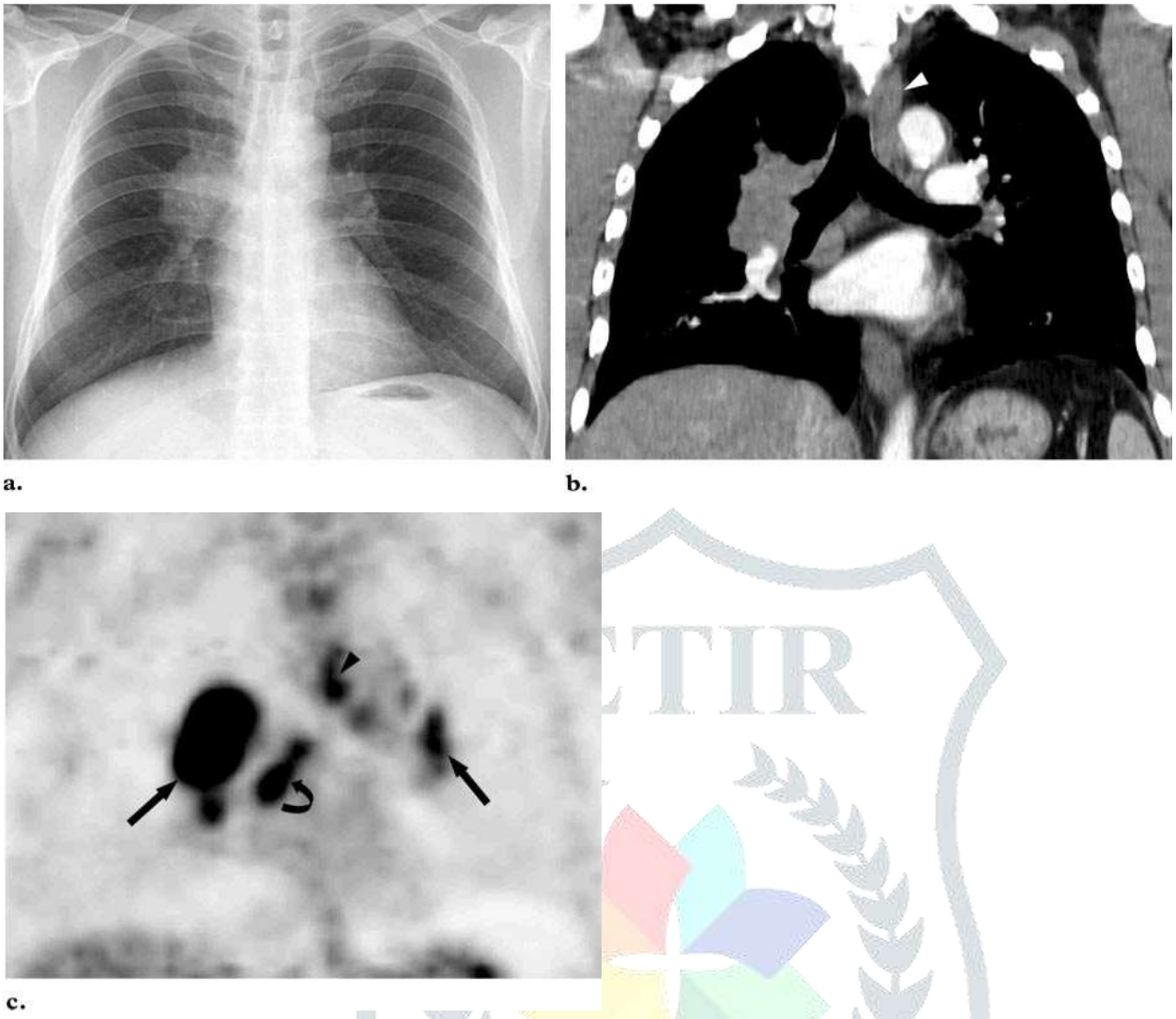

Figure 20. SCLC (a) Chest x-ray reveals pulmonary hilum bilateral extension. (b) The CT (2,5-mm segment thickness) enhanced coronal contrast scan reveals the right hilarium and left upper mediastinal (arrown) lymph nodes expansion. (c) The Coronal PET picture reveals a high FDG absorption in hilar (straight arrow) bilateral, subcarinal (curved) and the lymph nodes left paratracheal.

Figure 21. SCLC (a) Axial-contrast improved CT (5.0-mm segment thickness) scans acquired at the aortic arch stage reveal swollen lymph nodes in areas of extracapsular penetration in the right paratracheal arrows and bilational pre-pregnant areas. (b) the CT scan at the right middle lobar bronchial levels is seen by swollen (arrow) subcarinal and right hilar lymph nodes (arrowhead).

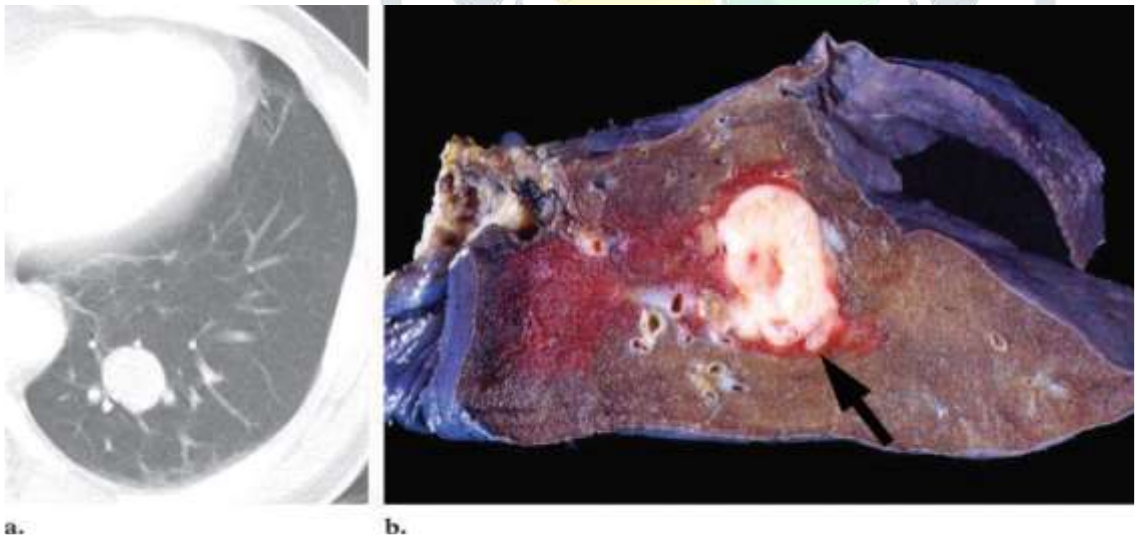

Figure 22. SCLC in periphery. (a) The axial CT scan of the ventricles reveals a 22 mm diameter nodule with a well defined margin in the lower left loben at the level of the ventricles, with a thickness of 5.0 mm. (b) The white stable nodule reveals the picture of the gross specimen (arrow).

References

Battafarano, R. J., Fernandez, F. G., Ritter, J., Meyers, B. F., Guthrie, T. J., Cooper, J. D., & Patterson, G. A. (2005). Large cell neuroendocrine carcinoma: an aggressive form of non-small cell lung cancer. The Journal of thoracic and cardiovascular surgery, 130(1), 166-172.

Baxi, A. J., Chintapalli, K., Katkar, A., Restrepo, C. S., Betancourt, S. L., & Sunnapwar, A. (2017). Multimodality imaging findings in carcinoid tumors: A head-to-toe spectrum. Radiographics, 37(2), 516-536.

Benson, R. E., Rosado-de-Christenson, M. L., Martínez-Jiménez, S., Kunin, J. R., & Pettavel, P. P. (2013). Spectrum of pulmonary neuroendocrine proliferations and neoplasms. Radiographics, 33(6), 1631-1649.

Caplin, M. E., Baudin, E., Ferolla, P., Filosso, P., Garcia-Yuste, M., Lim, E., ... & Zheng-Pei, Z. (2015). Pulmonary neuroendocrine (carcinoid) tumors: European Neuroendocrine Tumor Society expert consensus and recommendations for best practice for typical and atypical pulmonary carcinoids. Annals of oncology, 26(8), 1604-1620.

Chong, S., Lee, K. S., Chung, M. J., Han, J., Kwon, O. J., & Kim, T. S. (2006). Neuroendocrine tumors of the lung: clinical, pathologic, and imaging findings. Radiographics, 26(1), 41-57.

Cueto, A., Burigana, F., Nicolini, A., & Lugnani, F. (2014). Neuroendocrine tumors of the lung: hystological classification, diagnosis, traditional and new therapeutic approaches. Current medicinal chemistry, 21(9), 1107-1116.

Dalpiaz, G., & Cancellieri, A. (2017). Alveolar Diseases. In Atlas of Diffuse Lung Diseases (pp. 163-201). Springer, Cham.

Detterbeck, F. C. (2010). Management of carcinoid tumors. The Annals of thoracic surgery, 89(3), 998-1005.

Faggiano, A., Ferolla, P., Grimaldi, F., Campana, D., Manzoni, M., Davi, M. V., ... & Colao, A. (2012). Natural history of gastro-entero-pancreatic and thoracic neuroendocrine tumors. Data from a large prospective and retrospective Italian epidemiological study: the NET management study. Journal of endocrinological investigation, 35(9), 817-823.

Ferlito, A., Silver, C. E., Bradford, C. R., & Rinaldo, A. (2009). Neuroendocrine neoplasms of the larynx: an overview. Head & Neck: Journal for the Sciences and Specialties of the Head and Neck, 31(12), 1634-1646.

Gallego, G. A., Villaamil, V. M., Puerta, A. C., Pulido, E. G., & Aparicio, L. A. (2012). Neuroendocrine Tumours of the Lung. Lung Diseases—Selected State of the Art Reviews. Shanghai, China: InTech China, 203-231.

Kalemkerian, G. P. (2011). Staging and imaging of small cell lung cancer. Cancer Imaging, 11(1), 253.

Katyal, S., Oliver III, J. H., Peterson, M. S., Ferris, J. V., Carr, B. S., & Baron, R. L. (2000). Extrahepatic metastases of hepatocellular carcinoma. Radiology, 216(3), 698-703.

Kim, Y. N., Lee, H. Y., Lee, K. S., Seo, J. B., Chung, M. J., Ahn, M. J., ... & Yi, C. A. (2012). Dual-energy CT in patients treated with anti-angiogenic agents for non-small cell lung cancer: new method of monitoring tumor response?. Korean journal of radiology, 13(6), 702.

Lee, Y. J., Cho, A., Cho, B. C., Yun, M., Kim, S. K., Chang, J., ... & Kim, J. H. (2009). High tumor metabolic activity as measured by fluorodeoxyglucose positron emission tomography is associated with poor prognosis in limited and extensive stage small-cell lung cancer. Clinical cancer research, 15(7), 2426-2432.

Linning, E., Lu, L., Li, L., Yang, H., Schwartz, L. H., & Zhao, B. (2019). Radiomics for classifying histological subtypes of lung cancer based on multiphasic contrast-enhanced computed tomography. Journal of computer assisted tomography, 43(2), 300.

Miyoshi, T., Umemura, S., Matsumura, Y., Mimaki, S., Tada, S., Makinoshima, H., ... & Tsuchihara, K. (2017). Genomic profiling of large-cell neuroendocrine carcinoma of the lung. Clinical Cancer Research, 23(3), 757-765.

Modlin, I. M., Lye, K. D., & Kidd, M. (2003). A 5-decade analysis of 13,715 carcinoid tumors. Cancer: Interdisciplinary International Journal of the American Cancer Society, 97(4), 934-959.

Park, C. M., Goo, J. M., Lee, H. J., Kim, M. A., Lee, C. H., & Kang, M. J. (2009). Tumors in the tracheobronchial tree: CT and FDG PET features. Radiographics, 29(1), 55-71.

Rekhtman, N. (2010). Neuroendocrine tumors of the lung: an update. Archives of Pathology and Laboratory Medicine, 134(11), 1628-1638.

Saoud, M., Patil, M., Dhillon, S. S., Pokharel, S., Picone, A., Hennon, M., ... & Harris, K. (2016). Rare airway tumors: an update on current diagnostic and management strategies. Journal of thoracic disease, 8(8), 1922.

Stinchcombe, T. E., & Gore, E. M. (2010). Limited-stage small cell lung cancer: current chemoradiotherapy treatment paradigms. The oncologist, 15(2), 187.

Taal, B. G., & Visser, O. (2004). Epidemiology of neuroendocrine tumours. Neuroendocrinology, 80(Suppl. 1), 3-7.

Travis, W. D. (2010). Advances in neuroendocrine lung tumors. Annals of Oncology, 21, vii65-vii71.

Travis, W. D. (2014). Pathology and diagnosis of neuroendocrine tumors: lung neuroendocrine. Thoracic surgery clinics, 24(3), 257-266.

Tsuta, K., Raso, M. G., Kalhor, N., Liu, D. D., Wistuba, I. I., & Moran, C. A. (2011). Histologic features of low-and intermediate-grade neuroendocrine carcinoma (typical and atypical carcinoid tumors) of the lung. Lung Cancer, 71(1), 34-41.

Valente, M., Catena, L., Milione, M., Pusceddu, S., Formisano, B., & Bajetta, E. (2010). Common diagnostic challenges in the histopathologic diagnosis of neuroendocrine lung tumors: A case report. Case reports in oncology, 3(2), 202-207.

Volante, M., Brizzi, M. P., Faggiano, A., La Rosa, S., Rapa, I., Ferrero, A., ... & Papotti, M. (2007). Somatostatin receptor type 2A immunohistochemistry in neuroendocrine tumors: a proposal of scoring system correlated with somatostatin receptor scintigraphy. Modern Pathology, 20(11), 1172-1182.

Valli, M., Fabris, G. A., Dewar, A., Hornall, D., & Sheppard, M. N. (1994). Atypical carcinoid tumour of the lung: a study of 33 cases with prognostic features. Histopathology, 24(4), 363-369.

Zhang, G., Li, M., & Zheng, X. (2018). Case Discussion. In Early-stage Lung Cancer (pp. 291-413). Springer, Singapore.